Ψ-PIV: A novel framework to study unsteady microfluidic flows

Kislaya, Ankur; Deka, Antaran; Veenstra, Peter; Tam, Daniel; Westerweel, Jerry

Important note
To cite this publication, please use the final published version (if applicable).
Please check the document version above.

Ψ-PIV: A novel framework to study unsteady microfluidic flows

Ankur Kislaya[1, *], Antaran Deka[1], Peter Veenstra[2], Daniel S.W. Tam[1], Jerry Westerweel[1]

1: Laboratory of Aero- & Hydrodynamics, Delft University of Technology, the Netherlands
2: Shell Technology Centre Amsterdam (STCA), the Netherlands
* Correspondent author: a.kislaya@tudelft.nl

Keywords: PIV processing, Micro PIV, Microfluidics, stream-function, streamline, unsteady laminar flow

ABSTRACT

In micro-PIV, reaching the optimum image density has always been difficult due to high displacement gradient, coagulation of particles at the inlet and due to particles adhering to the surface to name a few. The most widely used method is to take ensemble correlation average of multiple PIV images to extract the velocity field. However, this leads to low temporal resolution. Hence, a method with high temporal resolution is pivotal to study unsteady laminar flow in microfluidic application. This work aims at developing a new PIV algorithm which reduces the effective seeding density and at the same time yield similar if not higher SNR compared to conventional PIV. We call this algorithm Ψ-PIV. This method is suitable for steady and unsteady laminar flows which are generally found in microfluidic applications. The reliability and the precision of the new method as a function of particle image pairs is investigated by synthetic image analysis. The main advantage of Ψ-PIV is its ability to achieve higher temporal resolution from the typical micro-PIV raw images. The experimental investigation for the flow around a 2D cylinder in a Hele-Shaw cell showed that the Ψ-PIV results in a reduction by approximately a factor of 25 in the number of frames required compared to conventional PIV.

1. Introduction

In micro-scale application, Particle image velocimetry (PIV) is generally referred to as micro-PIV (Santiago et al. [1998]; Meinhart et al. [1999]). The length scales of microfluidic device in the stream-wise and span-wise directions of the flow are considerably larger compared to the channel height in the wall normal direction. Hence, the Hele-Shaw cell conditions are valid for such devices.

The Poiseuille flow profile in the gap between two plates of a Hele-Shaw cell causes wall-normal variation of the flow velocity where fluid in the centre-line travels faster than the fluid near the walls. Large field-of-view results in large depth-of-field in the measurement volume. PIV yields low signal-to-noise ratio (SNR) due to the variation of the velocity along the depth-of-field and low seeding density. To reduce the effect of velocity gradient on the SNR, an enormous amount of tracer particles is required which is not feasible.

Meinhart et al. [2000] showed that the ensemble correlation of the image pairs substantially improves the SNR. Taking ensemble correlation average essentially increases the effective image density to determine the velocity field. However, this method leads to significant loss in instantaneous information. Ehyaei and Kiger [2014] from synthetic image simulation showed that a likelihood of 94% valid vectors can be reached if an aggregate of maximum displacement (Δx_{max}) and neighbouring displacements (Δx_{max}-1 ,Δx_{max}-2) are taken as valid vectors. Nonetheless, this does not give a reliable sub-pixel estimation of the particle displacement. It was shown by Kloosterman et al. [2011] that the measured PIV velocity can under-estimate upto 25% of the maximum Poiseuille flow velocity. Streamline image velocimetry by Keinan et al. [2013] uses long exposure images to capture path lines of the particle in fully developed laminar flow and determine velocity field from the fact that the volumetric flow rate in stream tube is conserved in low Reynolds number. The drawback of this method is its inability to measure velocity field in unsteady laminar flow cases.

This work focuses on determining the velocity field by reducing the image density and taking the advantage of the potential flow theory. Thus, making the current work relevant for measuring flow fields in steady and unsteady laminar flow. Quantitative analysis by means of PIV for large field-of-view is done in this investigation.

Theoretical description

The correlation peak for Poiseuille flow under low number of frames and/or less image density splits up into multiple peaks, although the particles in the interrogation area follows the flow direction. Fig. 1a shows the top-view of the correlation map for 2700 averaged images, where the smeared peak is at an angle of $63°$ *w.r.t* the x-axis. The corresponding normalized correlation function is shown in Fig. 1c. For the same interrogation window, the top view of the correlation map for 40 averaged image is shown in Fig. 1b. In this case, multiple peaks are present but it can be seen that the strong peaks are in the flow direction. The corresponding normalized correlation function along the $63°$ direction is shown in Fig. 1d which clearly shows multiple peaks.

This section describes a PIV algorithm which reduces the effective seeding density and yield similar if not higher SNR compared to conventional PIV. We call this algorithm "Ψ-PIV". Fig. 2 shows a flowchart describing the processing steps taken by Ψ-PIV. Consider a case where conventional micro-PIV requires an ensemble average of correlation plane of around 1000 frames to get the correct velocity field due to low seeding density and variation of the in-plane motion over the channel height. In case of Ψ-PIV, first the direction of the flow is determined from the correlation plane for all the interrogation areas (shown as dashed arrows in Fig. 2). The cross-

(a) Correlation map: 2700 frames

(b) Correlation map: 40 frames

(c) Correlation function: 2700 frames

(d) Correlation function: 40 frames
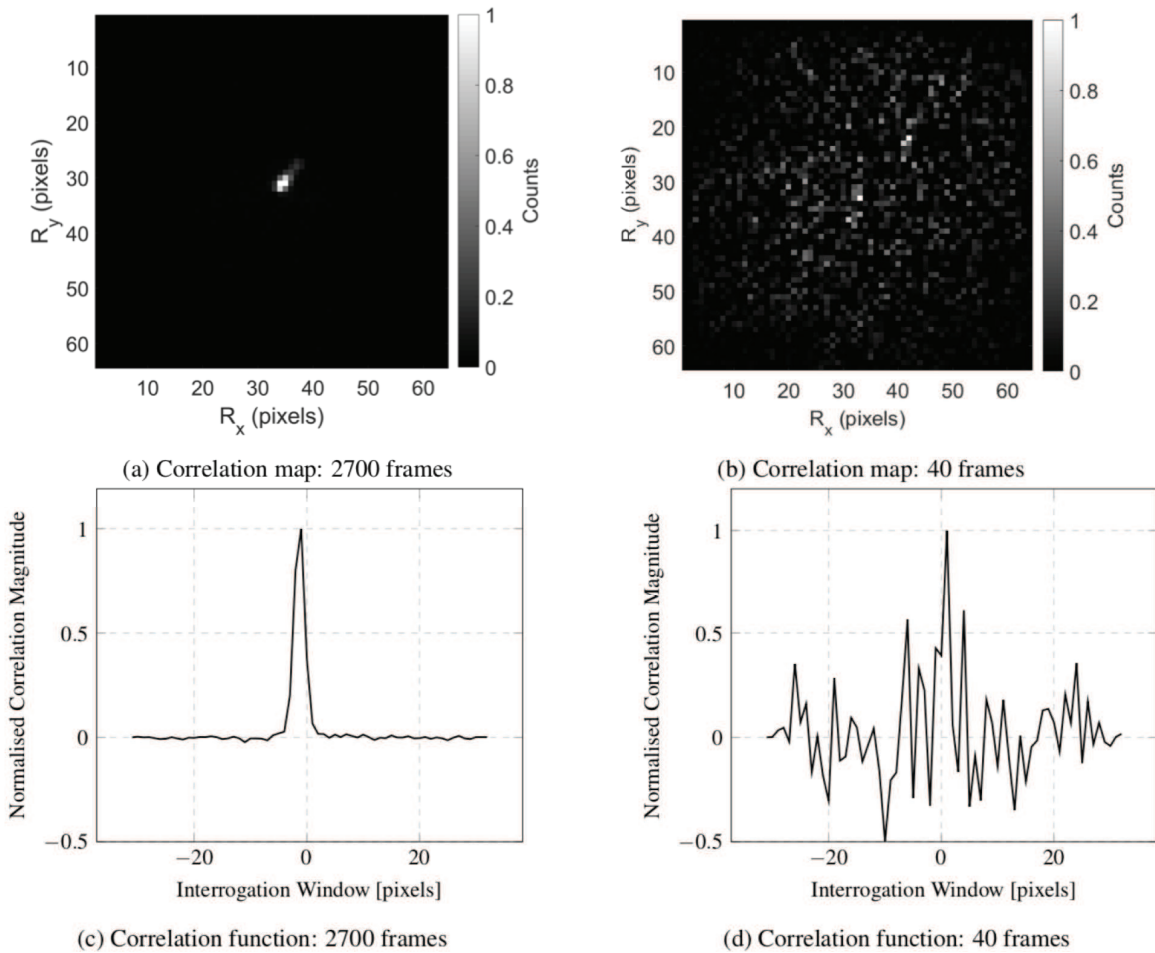
Fig. 1 Ensemble cross-correlation for 32 x 32 px interrogation window where the flow direction was calculated as 63° for 2700 averaged images & 40 averaged images.

correlation gives the highest peak in the direction in which the fluid is moving even with a fewer number of frames and with lower seeding density. Next, virtual particles are advected using a Runge-Kutta 4th order scheme through the interrogation areas. The path taken by the advection of the virtual particles are considered as streamlines. For simplicity, the flow is considered to have a uniform flow at the inlet, each streamline can be given a constant value at the inlet. In this way, the stream function from the (instantaneous) streamline pattern can be assigned.

The stream function (Ψ) is calculated for the centre location of each interrogation window by interpolating the nearest streamline values. Finally, using Eq. 1 the velocity components in x- and y- direction are calculated.

$$U = \left(\frac{\partial \Psi}{\partial y}\right), \; V = -\left(\frac{\partial \Psi}{\partial x}\right) \qquad\qquad (1)$$
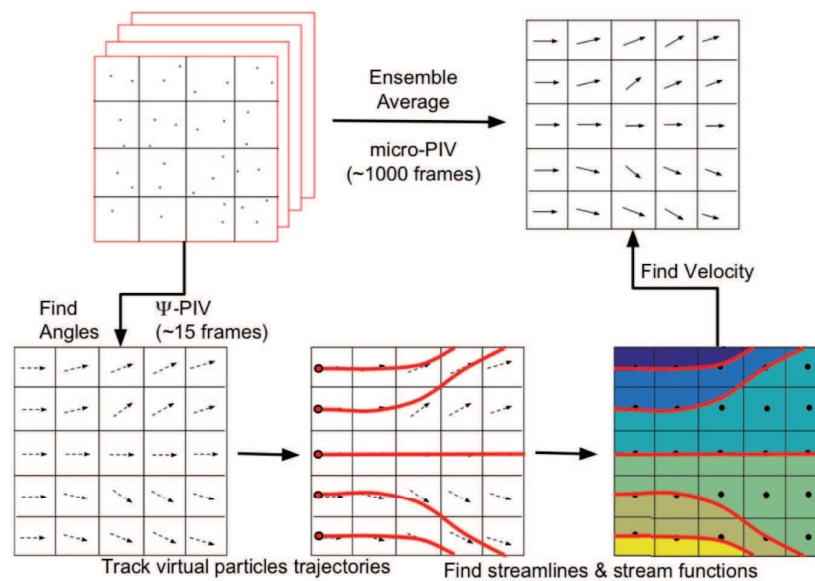
Fig. 2 Principal difference between PIV & Ψ-PIV algorithm

Validation

Synthetic images were generated in order to validate the Ψ-PIV algorithm. The images were made to mimic the uniform flow in span-wise direction under Hele-Shaw conditions. Thus, by randomly distributing the particles across the channel height leads to variability in velocity field for the uniform flow. Secondary effects such as Brownian motion and background noise from the image sensor are not taken into account for simplicity. The tracer particles in the image domain are re-inserted at random positions at the in-flow boundary in order to keep the image density constant across all frames. All images are generated with image size of 1024×1024 pixels with mean particle image diameter of 3 pixels. The centre-line displacement for the Poiseuille flow profile is 8 pixels. The processing of the synthetic images was done using single-pass FFT cross-correlation. The interrogation windows of 32×32 pixels with no overlap was chosen.

The valid detection probability shows the probability of determining the displacement peak correctly compared to the tallest random peak. Keane and Adrian [1990] showed that probability of determining true displacement peaks improves as the average number of particle pair in the interrogation area increases. In conventional PIV, the general guideline for having valid detection probability greater than 95%, NIF_IF_O of 8-10 particles for uniform flow test case is desired (Keane and Adrian [1992]; Adrian and Westerweel [2010]). In this case, the flow is in the channel between the two plates and volume illumination is used. Hence, there is no out-of-plane motion *i.e* F_O =1.
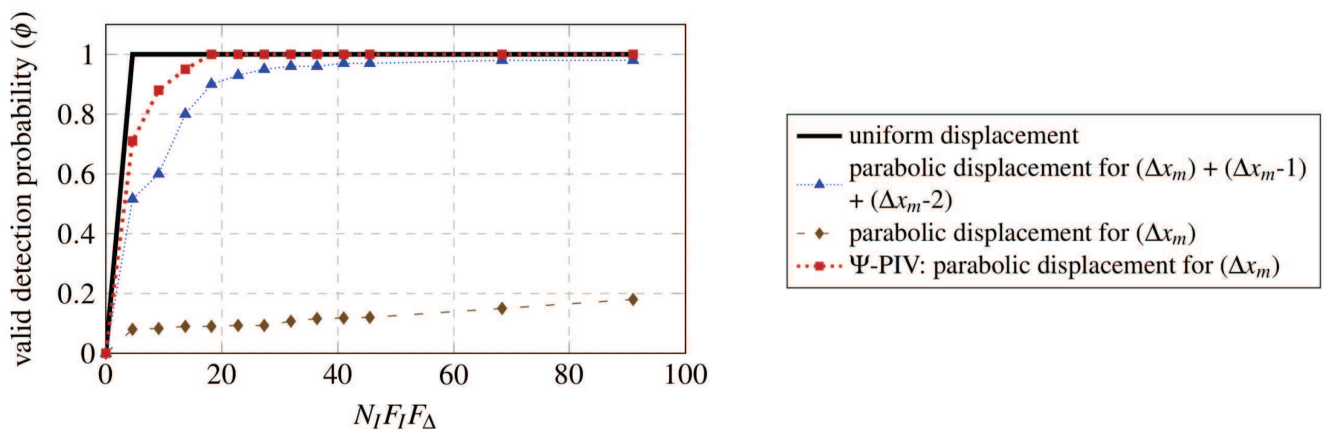
Fig. 3 The detection probability for the displacement correlation peak as a function of mean number of particle within an interrogation window and compared with the results of uniform displacement.

However, there is a loss-of-correlation due to in-plane displacement gradient of Poiseuille flow. Henceforth, $NI\ FI\ F_\Delta$ will be used for valid detection probability analysis (F_Δ represents correlations loss due to displacement gradient). Fig. 3 shows the valid detection probability as a function of effective image density ($NI\ FI\ F_\Delta$) for the synthetic data. For uniform displacement case, the probability of finding the true peak reaches 1 around $NIFIF_\Delta \approx 8$ as mentioned above. For parabolic flow, by considering peaks at location Δx_m, $\Delta x_m -1$ and $\Delta x_m -2$ to calculate the signal-to-noise ratio as shown by Ehyaei and Kiger [2014], a likelihood of 0.95 was reached. As multiple peaks are selected, this leads to ambiguity in the measured velocity field. Valid detection probability calculated for measured displacement (Δx_m) of Parabolic displacement shows poor performance. This is due to the particle size biasing effect where the maximum peak is located at 1 pixel less than the true displacement value (Ehyaei and Kiger [2014]). In case of Ψ-PIV, the valid detection probability reaches 1 substantially quicker due to the fact that less image density is required to determine the flow direction.

Experiment Setup

The PIV measurement was carried out in a Hele-Shaw cell consisting of two plexi-glass plates with length and breadth of 300mm and 100mm respectively. The two plates are separated by spacers of 500μm and are clamped on the edges to keep the gap constant throughout the channel length. A cylinder of diameter 30mm and thickness 500μm is placed on the centre-line along the width of the bottom plate at a
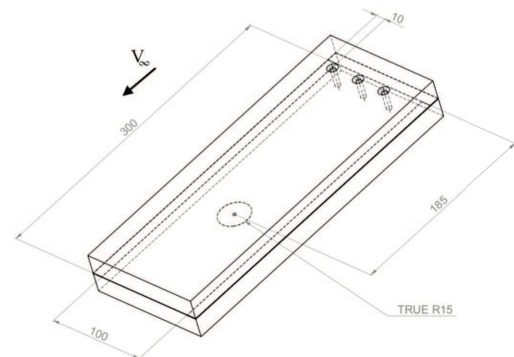
Fig. 4 Schematic of the test setup showing the flow direction & the three inlet holes

(a) Conventional PIV: 217 frames

(b) Conventional PIV: 9 frames

(c) Ψ-PIV: 9 frames
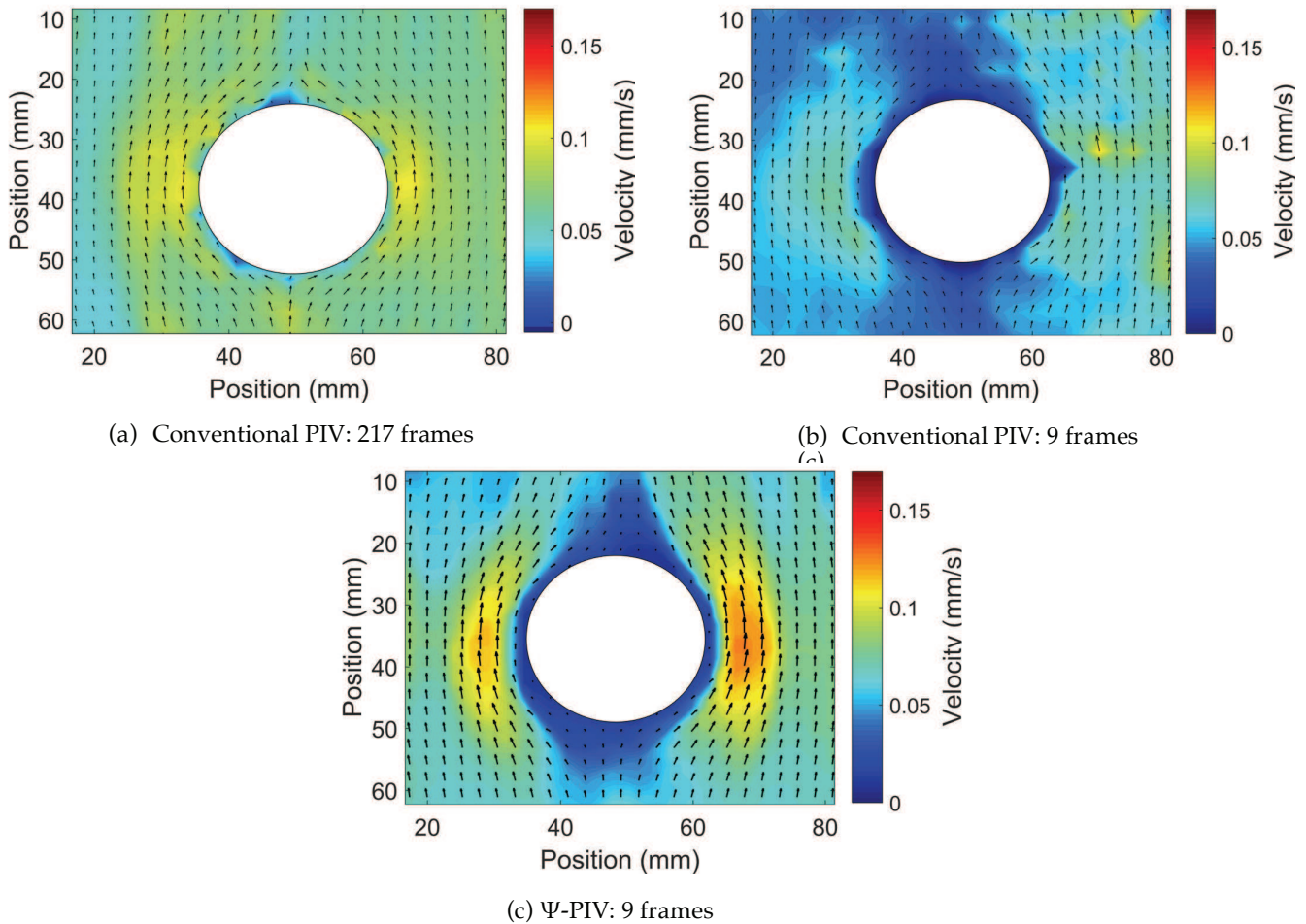
Fig. 5 Results of flow around a cylinder in a Hele-Shaw cell

distance of 180mm from the upstream cell edge. Cetoni neMESYS pump was used to generate pressure-driven flow with a centre-line velocity of 0.06mm/s, which yields a Reynolds number of 12. Water was seeded with mono-dispersed polystyrene microspheres with a mean diameter of 180μm-200μm (Cospheric). Images were recorded from LaVisions Imager Intense camera (CCD, 12-bit 1376×1,040pixels, pixel pitch 6.45μ m). The camera was equipped with a Nikon objective of 35 mm focal length. The magnification factor was 0.2. The active sensor size was cropped to 992×992 pixels. The f-stop was kept at 8 (depth of field = 1mm) to ensures that all the particles within the channel height are in focus. Acquisition frequency of 2Hz was used to acquire images.

Result

The PIV processing is done by single-pass cross-correlation with interrogation windows of 32×32pixel with 0% overlap. Fig. 5a shows the velocity field result from correlation average of 217 frames. The velocity direction is from bottom to top. The velocity near the boundary of the cylinder

decreases because Hele-Shaw condition is no longer valid near the wall. The Hele-Shaw condition only applies when the in-plane dimension (L) is much greater than the channel height (h) *i.e.* L ≫ h. Hence, the velocity decreases near the wall where distance is $O(h)$. Fig. 5b shows the velocity field with correlation average of 9 frames. The velocity vectors are not well resolved because seeding density is too low for correlation averaging to give a realistic outcome. Fig. 5c shows the velocity field for Ψ-PIV with 9 frames. The result is in close agreement with the PIV results from 217 averaged images (Fig. 5a). The increase in the velocity near the cylinder wall is better captured by Ψ-PIV compared to PIV with the same number of frames.
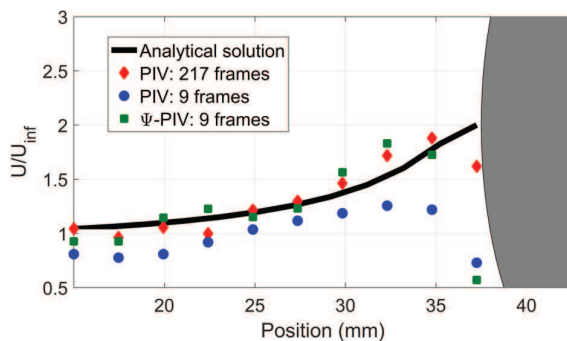
Fig. 6 Measured velocity distribution by PIV, Ψ-PIV around a cylinder (grey shaded region shows the left edge of the cylinder) and compared with the theoretical distribution which is calculated assuming ideal flow conditions

A quantitative comparative study of the velocity field from analytically, PIV and Ψ-PIV are shown in Fig. 6. The velocity field is made non-dimensional w.r.t. free stream. The analytic solution is calculated using the inviscid potential flow theory, hence there is a slip velocity on the edge of the cylinder. PIV result of 217 frames shows that the velocity field is in close agreement with the analytic solution except near the cylinder's edge because Hele-Shaw condition is violated. Hence the data point closest to the edge of the cylinder would not be considered for comparison. PIV result from 9 frames is clearly under-predicted due to low image density. Ψ-PIV result for 9 frames noticeably matches the PIV result of 217 frames. For Ψ- PIV, maximum difference in measured velocity with respect to reference velocity is 0.2 throughout the velocity distributions whereas for PIV with 9 frames the maximum difference is 0.8 throughout the velocity distribution *w.r.t* reference velocity. This shows the improvement in velocity field by Ψ-PIV measurement alongside lower frame requirement.

Discussion

The comparative study between PIV and Ψ-PIV (Fig. 3) shows that Ψ-PIV furnishes valid detection probability of more than 0.95 with effective image density of around 20 particle image pairs in an interrogation area. This means that either the seeding density needs to be high enough to take time resolved data or the ensemble average of few frames needs to be taken if the seeding density is low. To measure the angle precisely, the time separation between two frames should be

calculated such that the in-plane displacement is more than the particle image diameter for unambiguity.

This method is only valid for microfluidic flows because at high Reynolds number, potential flow theory is not valid and the method fails. To assign the stream function values to each point in the image domain, the streamlines in the upstream of the image should either be parallel to each other *i.e.* uniform flow or the stream-function value should be calculated analytically and those values should be assigned at the inlet of the image domain. Currently, angles are calculated using single cross-correlation technique. The required image density for determining angle can be lowered further by using adaptive windows technique and multigrid approach.

Conclusion

This paper describes a new method to determine the vector fields by reducing the image density compared to conventional micro-PIV technique. Ψ-PIV requires lesser image density to determine the angle at every interrogation window compared to high image density requirement of micro-PIV to determine the actual displacement vector. Once the direction is determined, potential flow theory is used to extract the velocity field. Synthetic image evaluation showed a valid detection probability of 0.95 for image density of 20 particles. A reduction in number of frames by a factor of 25 was shown from the experiment of flow around a 2D cylinder in a Hele-Shaw cell. High temporal resolution can be achieved by Ψ-PIV which makes it possible to retrieve instantaneous information from the measurement.

Reference

Adrian, R. and J. Westerweel (2010). *Particle image velocimetry*. Cambridge University Press.

Delnoij, E., J. Westerweel, G. Deen, A. Kuipers, and W. Swaaij (1999). Ensemble correlation PIV applied to bubble plumes rising in a bubble column. *Chemical Engineering Science 54*(21), 5159–5171.

Ehyaei, D. and K. Kiger (2014). Quantitative velocity measurement in thin-gap Poiseuille flow. *Experiments in Fluids 55*, 1–12.

Keane, R. and R. Adrian (1990). Optimization of particle image velocimeters. Part 1: Double pulsed systems. *Measurement Science and Technology 1*, 1202–1215.

Keane, R. and R. Adrian (1992). Theory of cross-correlation analysis of PIV images. *Applied Scientific Research 49*, 191–215.

Keinan, E., E. Ezra, and Y. Nahmias (2013). Frame rate free image velocimetry for microfluidic devices. *Applied Physics Letters 103*.

Kloosterman, A., C. Poelma, and J. Westerweel (2011). Flow rate estimation in large depth-of-field micro- PIV. *Experiments in Fluids 50*, 1587–1599.

Meinhart, C., S. Wereley, and M. Gray (2000). Volume illumination for two-dimensional particle image velocimetry. *Measurement Science and Technology 11*, 809–814.

Meinhart, C., S. Wereley, and J. Santiago (1999). PIV measurement of a microchannel flow. *Experiments in Fluids 27*, 414–419.

Meinhart, C., S. Wereley, and J. Santiago (2000). A PIV Algorithm for Estimating Time-Averaged Velocity Fields. *J. Fluids Eng 122*, 285–289.

Santiago, J., S. Wereley, C. Meinhart, D. Beebe, and R. Adrian (1998). A particle image velocimetry system for microfluidics. *Experiments in Fluids 25*, 316– 319.

Scarano, F. and M. Riethmuller (2000). Advances in iterative multigrid PIV image processing. *Experiments in Fluids 29*, s51–s60.